Unusual High Thermal Stability within a Series of Novel Lanthanide TATB Frameworks: Synthesis, Structure, and Properties (TATB = 4,4′,4″-s-Triazine-2,4,6-triyl-tribenzoate)

ARTICLE *in* CRYSTAL GROWTH & DESIGN · JANUARY 2012

Impact Factor: 4.89 · DOI: 10.1021/cg2008655

8 AUTHORS, INCLUDING:

Zhang Huabin
Chinese Academy of Sciences
49 PUBLICATIONS **468** CITATIONS
SEE PROFILE

Chongbin Tian
Chinese Academy of Sciences
36 PUBLICATIONS **407** CITATIONS
SEE PROFILE

CRYSTAL GROWTH & DESIGN

Article

pubs.acs.org/crystal

Unusual High Thermal Stability within a Series of Novel Lanthanide TATB Frameworks: Synthesis, Structure, and Properties (TATB = 4,4′,4″-s-Triazine-2,4,6-triyl-tribenzoate)

Huabin Zhang,[†,‡] Ning Li,[§] Chongbin Tian,[†,‡] Tianfu Liu,[†] Fenglei Du,[†,‡] Ping Lin,[†] Zhihua Li,[†] and Shaowu Du*[,†]

[†]State Key Laboratory of Structural Chemistry, Fujian Institute of Research on the Structure of Matter, Chinese Academy of Sciences, Fuzhou, Fujian 350002, P. R. China

[‡]Graduate University of Chinese Academy of Sciences, Beijing 100039, P. R. China

[§]Beijing National Laboratory for Molecular Sciences, State Key Laboratory of Rare Earth Materials Chemistry and Applications, College of Chemistry and Molecular Engineering, Peking University, Beijing 100871, P. R. China

Supporting Information

ABSTRACT: A series of multifunctional lanthanide-organic frameworks Ln(TATB)(H_2O) (Ln = Y **1**, Eu **2**, Gd **3**, Tb **4**, Dy **5**, Ho **6**, and Er **7**; TATB = 4,4′,4″-s-triazine-2,4,6-triyl-tribenzoate) with an unprecedented (4,8)-connected topology have been synthesized and characterized. The structures of these compounds were determined by single crystal X-ray diffraction and their thermal stability, sorption, as well as luminescent and magnetic properties were also investigated. Compounds **1**−**7** are isomorphic and present an open non-interpenetrated three-dimensional microporous framework constructed by infinite dinuclear-based, rod-shaped lanthanide-carboxylate secondary building units (SBUs) which arranged in nearly mutually perpendicular directions and interwoven by TATB linkers. All these compounds exhibit very high thermal stability and are stable up to 550 °C. The pore characteristics and gas sorption properties of these compounds were studied by experimentally measuring different gases (CO_2, N_2, and H_2) and different solvent molecules (H_2O and CH_3OH). The luminescent properties of compounds **1**−**7** in the solid state were investigated. The results show that **2** and **4** exhibited relatively high quantum yields and lifetime values, suggesting that they could be good candidates for light-emitting diodes (LEDs) and light applications. The variable-temperature magnetic studies show that the magnetic interaction between the Ln(III) ions in **2**−**7** was mainly due to the antiferromagnetic coupling as well as the depopulation of the Stark levels. The spin−orbit coupling parameter λ for Eu(III) (472 cm^{-1}) has been obtained for **2**. The in-phase and out-phase signals $\chi'_M T$ and χ''_M of **5** exhibit frequency dependence.

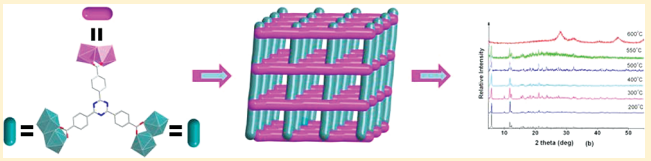

INTRODUCTION

Since 1990s, research interest in coordination polymers has been undergoing a vigorous period of exploration of their multidisciplinary applications thanks to the development of crystal engineering.[1−3] At present, increasing research effort has been intensively focused on the deliberate use of organic linkers to polymerize metal centers into multifunctional metal−organic frameworks (MOFs) with potentials of practical applications, ranging from molecular recognition and separation to gas storage and sensing.[4] As is well-known, one of the main concerns regarding these MOFs for practical applications is their thermal stability. Unfortunately, in contrast to traditional inorganic materials, for example, zeolites and others, only a few MOFs can retain their framework integrity at the temperatures up to 450 °C.[5] Therefore, the design and synthesis of MOFs with both multifunctionality and high thermal stability is a pursuit target for the chemists.

As functional metal centers, the technological importance of lanthanide metals have received more and more attention because of their various coordination geometries, peculiar luminescent and magnetic properties, as well as potential applications in gas adsorption, catalysts, and additives in metallurgy.[6] In particular, the luminescent and magnetic properties of lanthanide MOFs have been investigated widely during the past decade.[7] However, limited by the thermal stability, few MOFs have been put into practical applications.[8] Since it is usually accepted that the stability of the organic ligands and the compact networks of the host frameworks could play a crucial role in determining the thermal stabilities of MOFs, it is therefore possible to construct new multifunctional and high thermal stablility MOFs by selecting lanthanide metal ions and suitable organic ligands under proper reaction conditions.[8a,9]

Recently, the use of trigonal-planar 4,4′,4″-s-triazine-2,4,6-triyl-tribenzoate (TATB) with first-row transition metals to promote the formation of dinuclear and polynuclear secondary building units (SBUs) in porous MOFs has received great attention. Many porous MOFs with interesting SBUs, such as dinuclear paddle wheel,[10] trinuclear hourglass,[11] trinuclear μ_3-oxo-centered

Received: July 9, 2011
Revised: December 1, 2011
Published: December 15, 2011

Table 1. Pertinent Crystal Data and Structure Refinement Results for Compounds 1−7

compounds	1	2	3	4	5	6	7
formula	$C_{24}H_{14}N_3O_7Y$	$C_{24}H_{14}N_3O_7Eu$	$C_{24}H_{14}N_3O_7Gd$	$C_{24}H_{14}N_3O_7Tb$	$C_{24}H_{14}N_3O_7Dy$	$C_{24}H_{14}N_3O_7Ho$	$C_{24}H_{14}N_3O_7Er$
formula mass	545.28	608.35	613.63	615.30	616.87	621.30	623.63
space group	*Fddd*	*Fddd*	*Fddd*	*Fddd*	*Fddd*	*Fddd*	*Fddd*
a (Å)	22.128 (1)	22.252(4)	22.245(6)	22.200(4)	22.262(9)	22.154(9)	22.153(5)
b (Å)	28.524 (1)	28.629(5)	28.583(7)	28.614(2)	28.637(1)	28.577(1)	28.595(3)
c (Å)	29.033 (2)	29.191(5)	29.143(1)	29.122(9)	29.118(1)	29.053(1)	29.043(3)
V (Å^3)	18236.(18)	18596.(50)	18530.(10)	18500.(10)	18563.(13)	18394(12)	18398(20)
Z	32	32	32	32	32	32	32
D_c (g cm^{-3})	1.575	1.733	1.754	1.762	1.766	1.789	1.795
μ (mm^{-1})	2.60	2.75	2.91	3.11	3.28	3.49	3.70
F(000)	8704	9472	9504	9534	9824	9600	9632
GOF	1.03	1.05	1.03	1.04	1.16	1.17	1.36
R_1[a]	0.087	0.041	0.048	0.035	0.057	0.070	0.049
wR_2[a]	0.210	0.124	0.132	0.105	0.153	0.147	0.135

[a] $R = \sum(||F_o| - |F_c||)/\sum |F_o|$, $wR = \{\sum w[(F_o^2 - F_c^2)^2]/\sum w[(F_o^2)^2]\}^{1/2}$.

basic-carboxylate,[12] and tetranuclear μ_4-oxo-centered square-planar clusters[13] have been obtained. In these compounds, the planarity of TATB and its tendency to encourage $\pi-\pi$ stacking in MOFs prove an extraordinary ability to increase framework stability and a strong advantage in absorption and transformation of light energy, resulting in a preferential enhancement of luminescence. More recently, 2-fold interpenetrated and highly stable (up to 480 °C) three-dimensional (3D) MOFs (PCN-9) constructed by the connection of ytterbium and H_3TATB ligand was reported.[8] However, the interpenetration in PCN-9 increases the thermal stability at the expense of the reduction of the pore size and porosity, which is a disadvantage to the sorption properties. In this contribution, we have successfully synthesized a series of non-interpenetrated 3D lanthanide-organic frameworks Ln(TATB)(H_2O) (Ln = Y **1**, Eu **2**, Gd **3**, Tb **4**, Dy **5**, Ho **6** and Er **7**) built by rod-shaped SBUs which run through the whole framework in approximately mutually perpendicular directions. Such arrangement of SBUs, resembling "reinforcement cage", dramatically increases the thermal stability of these compounds and represents an important strategy for the generation of highly thermally stable MOF materials.

EXPERIMENTAL SECTION

Materials and Physical Measurements. All the chemicals were purchased commercially and used as received. Thermogravimetric experiments were performed using a TGA/NETZSCH STA449C instrument heated from 30−1200 °C (heating rate of 10 °C/min, nitrogen stream). The powder X-ray diffraction (XRD) patterns were recorded on crushed single crystals in the 2θ range 5−55° using Cu−Kα radiation. The XRD were measured on a PAN alytical X'pert PRO X-ray diffractometer. IR spectra using the KBr pellet technique were recorded on a Spectrum-One FT-IR spectrophotometer. Element analyses (C, H, and N) were measured with an Elemental Vairo EL III analyzer. H_2 and solvent molecules sorption measurements were performed with an Intelligent Gravimetric Sorption analyzer (IGA100B) and hydrogen storage analyzer (HTP1). The ASAP 2020 surface area analyzer was used to measure the N_2 and CO_2 adsorption isotherm. The samples were heated at 250 °C (heating rate 2 °C/min) under vacuum ~10^{-7} mbar for 12 h before the analysis was started. The polycrystalline magnetic susceptibility data were collected on a Quantum Design MPMS (SQUID)-XL magnetometer in the temperature range from 2 to 300 K. Fluorescence spectra for the solid samples were performed on an Edinburgh Analytical instrument FLS920.

Synthesis of [Ln(TATB)H_2O] (Ln = Y 1, Eu 2, Gd 3, Tb 4, Dy 5, Ho 6 and Er 7). In a typical reaction, a mixture of $Y(NO_3)_3{\cdot}6H_2O$ (0.25 mmol) and H_3TATB (0.15 mmol) were placed in a 20 mL of Teflon-lined stainless steel vessel with 6 mL of mixed-solvent of dimethyl sulfoxide (DMSO) and H_2O (V/V = 1:1). The mixture was heated to 120 °C in 4 h and kept to this temperature for 3 days. The reaction system was cooled slowly to room temperature during another 2 days. White prismatic crystals of **1** were obtained (yield 56% based on $Y(NO_3)_3{\cdot}6H_2O$). Elemental analysis calcd (%) for $C_{24}H_{14}N_3O_7Y$ (544.99): C 52.86, H 2.59, N 7.71; found: C 53.16, H 2.54, N 7.68. IR: 3389m, 1943w, 1563s, 1538s, 1358s, 1173m, 1015m cm^{-1}.

Colorless prismatic crystals of **2**−**5**, pink prismatic crystals of **6** and **7** were obtained in moderate yields (49%−66%) by a similar method as described for **1** except that the corresponding $Ln(NO_3)_3{\cdot}6H_2O$ were used instead of $Y(NO_3)_3{\cdot}6H_2O$. Elemental analysis calcd (%) for **2** $C_{24}H_{14}N_3O_7Eu$ (608.35): C 47.38, H 2.32, N 6.91; found: C 47.96, H 2.34, N 7.11. IR for **2**: 3390m, 1943m, 1563s, 1538s, 1358s, 1173m, 1016m cm^{-1}. Elemental analysis calcd (%) for **3** $C_{24}H_{14}N_3O_7Gd$ (613.62): C 46.98, H 2.30, N 6.85; found: C 46.59, H 2.29, N 6.70. IR for **3**: 3391m, 1944m, 1567s, 1505s, 1359s, 1173m, 1016m cm^{-1}. Elemental analysis calcd (%) for **4** $C_{24}H_{14}N_3O_7Tb$ (615.30): C 46.85, H 2.29, N 6.83; found: C 46.69, H 2.31, N 6.66. IR for **4**: 3390m, 1943m, 1563s, 1505s, 1360s, 1173m, 1015m cm^{-1}. Elemental analysis calcd (%) for **5** $C_{24}H_{14}N_3O_7Dy$ (618.88): C 46.58, H 2.28, N 6.79; found: C 45.13, H 2.26, N 6.68. IR for **5**: 3391m, 1944m, 1567s, 1505s, 1359s, 1173m, 1016m cm^{-1}. Elemental analysis calcd (%) for **6** $C_{24}H_{14}N_3O_7Ho$ (621.30): C 46.39, H 2.27, N 6.76; found: C 46.69, H 2.28, N 6.53. IR for **6**: 3389m, 1944m, 1568s, 1506s, 1359s, 1172m, 1016m cm^{-1}. Elemental analysis calcd (%) for **7** $C_{24}H_{14}N_3O_7Er$ (623.63): C 46.22, H 2.26, N 6.76; found: C 46.39, H 2.30, N 6.24. IR for **7**: 3390m, 1943m, 1563s, 1505s, 1360s, 1173m, 1015m cm^{-1}.

Crystal Structure Determination. Single-crystal X-ray diffraction data were collected on a Rigaku diffractometer with a Mercury CCD area detector (Mo Kα; λ = 0.71073 Å) at room temperature. Empirical absorption corrections were applied to the data using the Crystal Clear program.[14] The structures were solved by the direct method and refined by the full-matrix least-squares on F^2 using the SHELXTL-97 program.[15] Metal atoms in each compound were located from the *E*-maps, and other non-hydrogen atoms were located in successive difference Fourier syntheses. All non-hydrogen atoms were refined anisotropically. The organic hydrogen atoms were positioned geometrically, while those of the water molecules were located using the difference Fourier method and refined freely. Crystallographic data and other pertinent information for **1**−**7** are summarized in Table 1. Selected bond distances and angles for these compounds are listed in Table S1, Supporting Information. CCDC numbers for coordination polymers **1**−**7** are 827927−827933, respectively.

dx.doi.org/10.1021/cg2008655 | *Cryst. Growth Des.* 2012, 12, 670−678

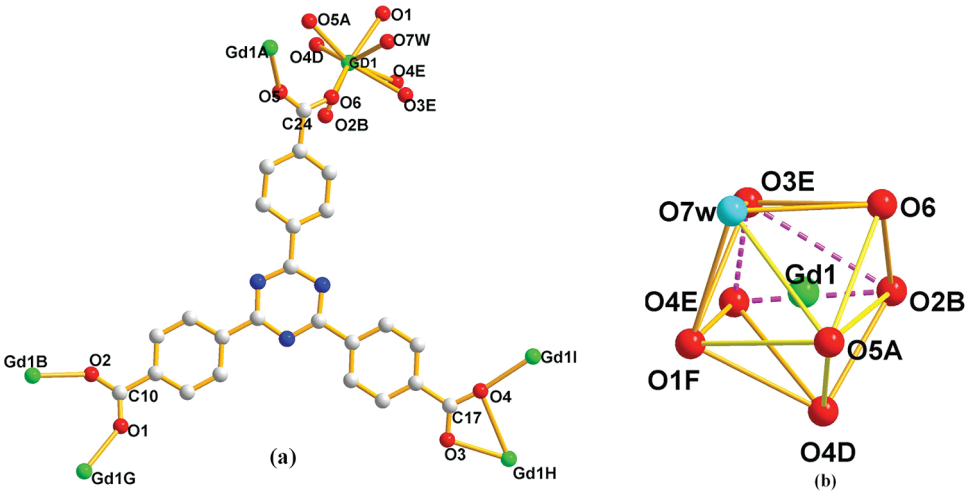

Figure 1. (a) Representation of the Gd(III) coordination environments and ligands' coordination modes of compound **3**. (b) Distorted dicapped trigonal-prismatic coordination polyhedron of the Gd(III). Symmetry codes (A) $-x + 1/4, y, -z + 1/4$; (B) $-x - 1/4, -y + 3/4, z$; (D) $x + 3/4, y - 1/4, -z$; (E) $-x, y + 1/4, z + 1/4$; (F) $-x + 9/4, y, -z - 3/4$; (G) $-x + 5/2, y + 1/4, z - 1/4$; (H) $x + 1/2, -y + 1/4, -z - 1/4$; (I) $-x + 1/2, -y + 1/2, -z$.

RESULTS AND DISCUSSION

Description of Crystal Structures. Single crystal X-ray analysis revealed that the seven MOFs are isostructural with each other and have noninterpenetrated open 3D frameworks built by infinite dinuclear-based, rod-shaped lanthanide-carboxylate SBUs and TATB linkers. Here, we select **3** as the representative example to describe the structures in detail. As shown in Figure 1, the asymmetry unit of **3** consists of one crystallographically unique Gd(III) ion, one $TATB^{3-}$ ligand, and one coordinated water molecule. Each Gd(III) ion coordinates to a water oxygen atom and seven carboxylic oxygen atoms from six $TATB^{3-}$ forming a distorted bicapped triprismatic coordination geometry. The Gd−O bond lengths vary from 2.323(6) to 2.486(4) Å. All the Ln−O distances are in the ranges compatible with the values of the previously published lanthanide compounds.[9] The TATB ligands are almost planar and appear in pairs by forming $\pi-\pi$ stacking in a staggered arrangement. The two triazine rings are stacked in such a way that the negatively charged nitrogen atoms are aligned with the positively charged carbon atoms from the other ring to maximize $\pi-\pi$ stacking, as observed in compounds based on tripyridyltriazine. The distance between the centers of the two triazine rings is 3.64 Å, which is comparable with typical $\pi-\pi$ stacking interactions between two phenyl rings (Figure S1, Supporting Information).[16] All the carboxylic groups are deprotonated and adopt two different bridging modes ($(\kappa^1-\kappa^1)-\mu_2$ and $(\kappa_2-\mu_2)-\mu_2$ modes) with the Gd(III) centers, resulting in the formation of gadolinium-carboxylate chains passing through the framework in two directions that are almost mutually perpendicular. Each infinite rod-shaped gadolinium-carboxylate chain can be regarded as a SBU, in which the neighboring gadolinium ions are alternately separated by 4.029(5) and 5.501(1) Å. These SBUs are sustained by rigid phenyl rings of TATB ligands to construct a 3D coordination framework (Figure 2). Up to now, several MOFs constructed from rod-shaped SBUs have been reported; in most of cases, the metal-carboxylate chains are along a single direction.[17] As far as our knowledge, **3** represents the first example of MOFs constructed through rod-shaped SBUs toward two staggered directions. The size of the void created by the formal removal

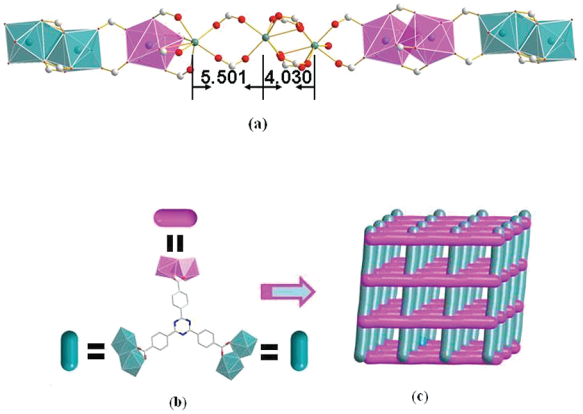

Figure 2. (a) Infinite dinuclear-based, rod-shaped lanthanide-carboxylate SBUs, (b) rod-shaped SBUs in two separate directions, and (c) the arrangement of rod-shaped SBUs running through the whole framework.

of the coordinated water molecules is 1870.6 $Å^3$, which is 10.1% of the unit cell volume.

From the topological point of view, the $TATB^{3-}$ can be defined as a four-connected node, while the Gd−O4−Gd dinuclear unit can be viewed as a eight-connected node. This net can be specified by the Schläfli symbol of $(4^4.6^2)_2(4^8.6^8.8^{12})$ and the vertex symbols for the two nodes (Gd_2, $TATB^{3-}$) being $[4.4.4.8_{30}.4.8_{42}]$ and $[4.4.4.4.4.4.4.4.6.6.6.6.6_2.8_2.8_4.8_6.8_8.8_8.8_{12}.8_{12}.8_{16}.8_{16}.8_{20}.8_{20}.8_{24}.8_{24}.8_{34}.8_{34}]$, respectively (Figure 3). It should be noted that structures incorporating high connected nodes remain highly unexplored.[18] A prominent structural feature of **3** is the observation of an unprecedented (4, 8)-connected network.

X-ray Diffraction (XRD) and Thermal Stability Analysis. The simulated and experimental XRD patterns of compounds **1**−**7** obtained at room temperature are shown in Figure S2, Supporting Information. Their peak positions correspond well with each other, indicating the phase purity of the solids. The difference in reflection intensities between the simulated and experimental patterns may be due to variation in the preferred

dx.doi.org/10.1021/cg2008655 | Cryst. Growth Des. 2012, 12, 670−678

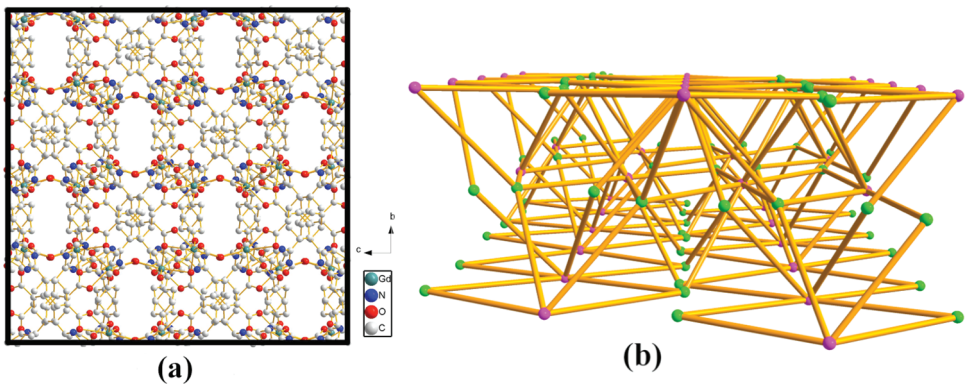

Figure 3. (a) 3D microporous framework of **3** viewed along the *bc* plane and (b) view of 3D architecture and (4, 8)-connected topological net of **3**.

orientation of the powder samples during collection of the experimental XRD data.

Thermogravimetric analysis (TGA) experiments were conducted to determine the thermal stability for the isomorphic **1**−**7** under nitrogen atmosphere in the temperature range of 30−1200 °C. TG analyses indicate that all these compounds have very high thermal stability and exhibit similar thermal behavior (Figures 4a and S3). Therefore, only the thermal

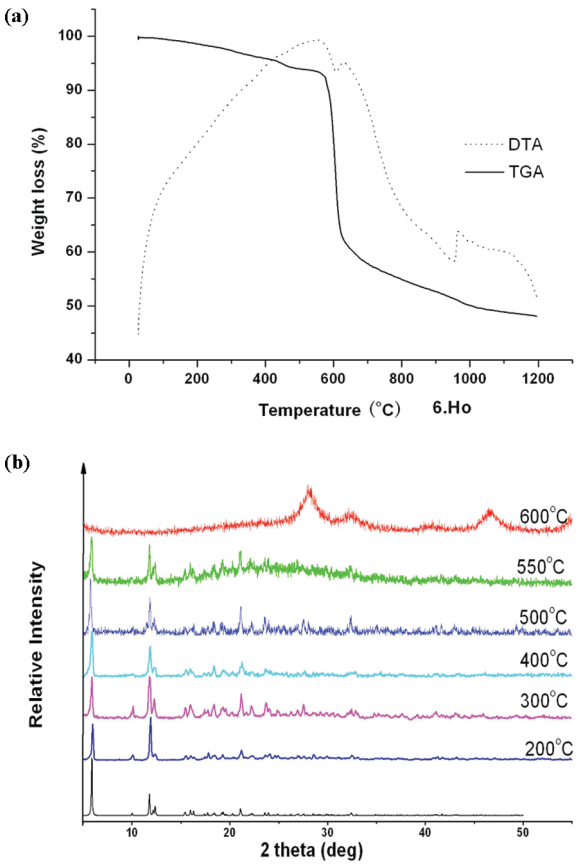

Figure 4. (a) TG and DTA curves for compounds **6·Ho**, (b) temperature-dependent PXRD patterns for **6**.

stability of **6** is discussed in detail. A first weight loss of 4.5% occurs from room temperature to 380 °C, which corresponds to the loss of coordinated water molecule, giving a free framework of Ho(TATB). After that, a plateau appears and the dehydrated sample is thermally stable up to 595 °C. The framework of Ho(TATB) starts to collapse with the loss of TATB ligands from 595 to 700 °C.

It is worth noting that compounds **1**−**7** still showed very good crystallinity at 550 °C. At 600 °C, the long-range order of the structures was lost and the amorphous phases were formed. These relative conclusions were corroborated by temperature-dependent XRD patterns of **6** which were conducted after calcination at elevated temperature in the range of 200−600 °C (Figure 4b). Generally speaking, degradation of the organic components of porous MOFs typically starts at moderate temperatures (200−350 °C),[5] leading to the decomposition of the frameworks. There are only limited porous MOFs which are reported to be stable above 500 °C,[8] unfortunately, few of them have accessible void space except some ZIFs reported recently by Zhang et al.[1g,19] To the best of our knowledge, the present series of compounds are the first carboxylate-based MOFs with both high thermal stability (over 550 °C in air) and porosity, which may highly facilitate their functional applications. It is assumed that in compounds **1**−**7**, the arrangement of rod-shaped SBUs in two directions tightens the backbone of the ligands and enhances their resistance to pyrolysis.

Adsorption Properties. The excellent framework stability with a void of 1870.6 Å^3 per unit cell provides an opportunity to establish permanent porosity and guest affinity depending upon the size and porosity of the different adsorbates. The CO_2 adsorption measurement at 273 K was carried out to check the porosity of compound **1**. As shown in Figure 5a, the CO_2 adsorption increases at the start of the experience and do not reach a plateau even at the end of experience, indicating the adsorption isotherm is not saturated under these conditions.[20] The adsorption isotherm data were fitted to the BET equation to give a surface area of 144.84 m^2/g (Langmuir 186.46 m^2/g), testifying the permanent porosity of **1**. The N_2 adsorption isotherm for **1** at 77 K shows no uptake by the framework, preferential CO_2 uptake over nitrogen might be attributed to a size exclusive effect in which the channels are accessible to CO_2, but not to N_2 because of their differential kinetic diameters of 3.46 and 3.64 Å.[21]

Vapor sorption studies of CH_3OH and H_2O were also conducted at room temperature. The CH_3OH adsorption represents type II isotherm with 4.46 wt % (1.3 mmol/g) at 298 K and P/P_0 = 1. The adsorption amount of water reached a plateau of 3.90 wt % (2.2 mmol/g) at P/P_0 = 0.6, which indicates that there is a diffusion of water molecules into the narrow pores (Figure 5b).[22] The observed hysteresis (Figure S4, Supporting Information) between the adsorption−desorption curves for

dx.doi.org/10.1021/cg2008655 | *Cryst. Growth Des.* 2012, 12, 670−678

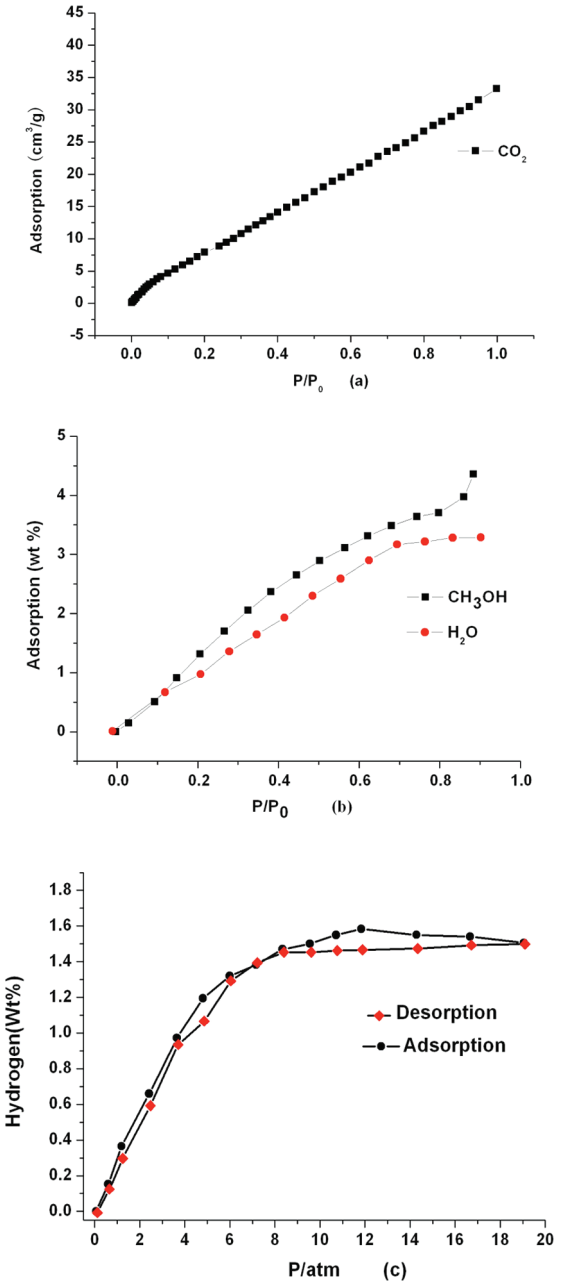

Figure 5. (a) CO_2 adsorption isotherm of **1** at 273 K and P/P_0 = 1. (b) CH_3OH and H_2O adsorption isotherms of **1** at 298 K and P/P_0 = 1. (c) H_2 adsorption/desorption isotherm of **1** at 77 K and 20 bar.

water and methanol may be attributed to the intercrystalline voids.[23]

Hydrogen adsorption isotherm reveals that **1** can store up 1.58 wt % (176 cm^3/g) hydrogen at 77 K and 20 atm. As shown in Figure 5c, the H_2 adsorption isotherm displays type I behavior with a steep uptake in the low temperature range indicating a strong affinity of hydrogen molecules toward pore surfaces.[24] This value is comparable to those of reported porous MOFs with moderate H_2 adsorption.[25]

Luminescent Properties. The luminescent properties of compounds **1**−**7** in the solid state were investigated and principally studied compounds **2** and **4**. Their solid-state excitation and emission spectra were measured at room temperature. The excitation spectra were monitored around the Ln(III) more intense emission lines, 614 nm for Eu(III) and 544 nm for Tb(III). It can be seen clearly that the excitation spectrum of **2** consists of a broadband and a weak line. The broadband below 350 nm is due to the charge-transfer between the O^{2-} and Eu(III) ions and $\pi \rightarrow \pi^*$ electron transition of the organic bridging ligands, while the weak line at 466 nm is attributed to the $^7F_0 \rightarrow {}^5D_2$ transitions (Figure 6a).

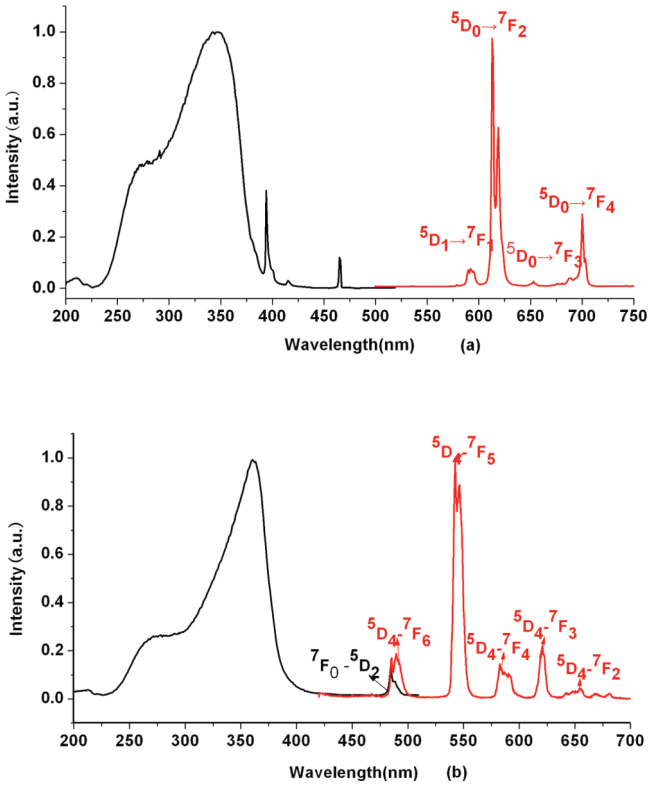

Figure 6. Solid-state excitation and emission spectra for **2** (a) and **4** (b) at room temperature.

The excitation spectrum of **4** (Figure 6b) displays a large broadband with a structured profile in the UV spectral region which is ascribed to the electronic transitions of organic ligands. In addition, an intra4f[8] line ascribed to the transitions between $^7F_0$ states and $^5D_2$ excited levels is observed. The absolute high intensity of the broadband compared to that of the intra4f^n lines indicates that the $\pi \rightarrow \pi^*$ electron transition of the organic bridging ligands is a dominant path to sensitizing Eu(III) / Tb(III) excited states.

As shown in Figure 6a, upon excitation at 350 nm, characteristic emissions associated with the 4f → 4f transitions of the $^5D_0$ excited state to the low-lying ^7F_J (J = 0, 1, 2, 3, and 4) levels of Eu(III) can be observed in the range 570−720 nm. Note that the $^5D_0 \rightarrow {}^7F_2$ transition of Eu(III) centered at 614 nm for **2** dominates the whole emission spectrum. Furthermore, it is well-known that the emissions of Eu(III) are usually employed as a sensitive probe to investigate the coordination and local environment around cations. The $^5D_0 \rightarrow {}^7F_2$ transition of Eu(III) is hypersensitive to site symmetry and of the electric-dipole (ED) nature, which is only permitted on the condition that Eu(III) occupies a site without an inversion center according to Judd-Ofelt theory.[26] By contrast, the $^5D_0 \rightarrow {}^7F_1$ transition is insensitive to site symmetry and the magnetic-dipole (MD) nature. The intensity ratio of $^5D_0 \rightarrow {}^7F_2$ to $^5D_0 \rightarrow {}^7F_1$ transitions of Eu(III) gives the information on the structure,

dx.doi.org/10.1021/cg2008655 | Cryst. Growth Des. 2012, 12, 670−678

such as the ligand environment and site symmetry. For **2**, the intensity of $^5D_0 \rightarrow {}^7F_2$ transition is much stronger than that of $^5D_0 \rightarrow {}^7F_1$. Moreover, the $^5D_0 \rightarrow {}^7F_0$ transition of Eu(III) is invisible in the emission spectrum, which is only allowed for Cs, Cn, and Cnv site symmetries according to the ED selection rule.[27] These experimental facts thus suggest that the Eu(III) ion in **2** is located at a high-symmetry site, which is in good agreement with our single-crystal X-ray analysis. Excited at 325 nm (Figure 6b), the emission spectrum of **4** shows green-luminescence with typical emission bands at 491, 545, 585, 622, 648, 670, and 680 nm, assigned to $^5D_4 \rightarrow {}^7F_J$ (J = 6−0) transitions. The dominant band of these emissions is attributed to the hypersensitive transition $^5D_4 \rightarrow {}^7F_5$ of Tb(III) ions, while the stronger luminescent band corresponds to $^5D_4 \rightarrow {}^7F_6$ transition, and the two less intense bands are ascribed to $^5D_4 \rightarrow {}^7F_4$ and $^5D_4 \rightarrow {}^7F_3$ transitions, respectively. The $^5D_4 \rightarrow {}^7F_J$ (J = 2−0) transitions are measured with weak intensity. It is worth noting that there is no apparent residual ligand-based emission in the 400−480 nm region, indicating an efficient energy transfer from ligand *p*-excited states to terbium *f*-excited states.

The emission quantum yields were measured at room temperature under the excitation wavelengths that maximize the emissions of lanthanide cations. As a result, the quantum yields are 19.89% for **2** and 1.36% for **4**. The luminescence decay curves of **2** and **4** were also obtained at room temperature (Figure S5, Supporting Information). The corresponding lifetime for **2** is about $\tau 1$ = 0.963 (100%) ms, and that for **4** is about $\tau 1$ = 3.916 (93.26%) ms and $\tau 2$ = 10.725 (6.74%) ms (determined by monitoring $^5D_0 \rightarrow {}^7F_2$ line excited at 350 nm and $^5D_4 \rightarrow {}^7F_5$ line excited at 325 nm, respectively). Compounds **2** and **4** both have a relatively long quantum yield and a luminescence lifetime, which are comparable to those observed for other related Eu(III) and Tb(III) compounds.[28] Because the excitations now fall in the range of those commercially available, they could be good candidates for light-emitting diodes (LEDs) and light applications.

Luminescence properties of MOFs can be dramatically affected by the coordination environment of metal centers, the species of guest molecules, and so forth.[29] In general, water molecules are very effective nonradiative relaxers to quench luminescence because of the loss of excited state energy from the Ln(III) ions through vibration energy of the close proximity OH oscillator. To further understand the effects of the water molecules on the luminescence properties of **2** and **4**, we investigated the quantum yields and lifetimes of their dehydrated samples. To ensure that the coordinated water molecules can be removed thoroughly upon the dehydrated process, samples of **2** and **4** were dehydrated at 450 °C for 2 h. Removal of the coordinated water molecules greatly changed the quantum yields and lifetimes. The quantum yields for dehydrated **2** and **4** are 27.24% and 1.82%, increasing about 36.95% and 33.82%; meanwhile, the luminescence lifetimes for dehydrated **2** and **4** were determined to be 1.296 and 6.493 ms, improved about 34% and 48%, respectively, in comparison with those for as-synthesized **2** and **4** (Table 2). These results thus confirm the conclusion that the direct coordination of water molecules on the lanthanide ions would reduce their fluorescent efficiency. To prevent the fluorescence quenching caused by the vibration of coordinated water molecules, low temperature decay lifetimes were measured at 10 and 77 K. However, no noticeable changes in lifetime were observed for **2** and **4**, probably due to the H_2O-induced oscillate which is very strong and fairly temperature insensitive.

Table 2. Quantum Yields and Lifetimes of the As-Synthesized and Dehydrated Phases of Compound 2 and 4

		lifetimes (*ms*)		
compound	experience condition	τ_1	τ_2	quantum yields
as-synthesized **2**	RT	0.963 (100%)		19.89
	77	0.958 (100%)		
	10	0.971 (100%)		
dehydrated **2**	RT	1.296 (100%)		27.24
as-synthesized **4**	RT	3.916 (93.26%)	10.725 (6.74%)	1.36
	77	3.761 (95.05%)	16.291 (4.95%)	
	10	3.819(96.07%)	14.759 (3.93%)	
dehydrated **4**	RT	4.946 (83.21%)	14.160 (16.79)	1.82

The emission spectra of compounds **1**, **3**, and **5**−**7** in the solid state are depicted in Figure S6, Supporting Information. For compound **5**, two peaks at 476 and 569 nm are assigned to the transition of $_4F^{9/2} \rightarrow {}_6H^{15/2}$ and $_4F^{9/2} \rightarrow {}_6H^{13/2}$ (Figure S6a, Supporting Information), respectively. No other compounds exhibit characteristic emission but broad emission bands at about 450 nm under the excitation of 340 nm; by comparing with the luminescence behavior of free H_3TATB ligand, we can draw a conclusion that the emissions for compounds **1**, **3**, **6**, **7** may be due to the intraligand transition ($\pi \rightarrow \pi^*$) and the mismatch of the triplet state energy level of the ligand with the energy levels of ligand with the energy levels of lanthanide ions. Interestingly, a self-absorption peak of **6** for Ho^{3+} at 456 nm is presented in the emission spectrum of compound **6** as shown in Figure S6b, Supporting Information, which might be owing to the overlap between the emission wavelength of ligand and the absorption wavelength of Ho^{3+} that locates at 456 nm corresponding the hypersensitive $^5I_8 \rightarrow {}^5G_6$ (ΔJ = 2) transition.[30]

Magnetic Properties. The temperature-dependent magnetic susceptibilities of **2**−**7** were measured in the temperature range of 2−300 K at 1000 Oe. For **2**, the value of $\chi_M T$ at 300 K is equal to 1.957 emu· K·mol^{-1} (Figure 7a), which is obviously smaller than the theoretical high-temperature limit ($(\chi_M T)_{HT}$ = 4.50 emu·K·mol^{-1}). It then decreases continuously because of the depopulation of Stack levels, reaching a value close to zero (0.040 emu·K·mol^{-1}) at 2 K, which corresponds to a nonmagnetic ground state of $^7F_0$ for Eu(III) ions. The $\chi_M T$ versus T data for **2** could also be analyzed on the basis of the equations deduced from the monomeric Eu(III) system with the free-ion approximation over the whole temperature range. The least-squares fitting of the $\chi_M T$ versus T curve leads to the spin−orbit coupling parameter, λ = 472(4) cm^{-1}, and the Weiss-like constant, θ = 1.67(17) K, with an agreement factor R of 2.7 × 10^{-4} ($R = \Sigma[(\chi_M T)_{obsd} - (\chi_M T)_{calcd}]^2/\Sigma(\chi_M T)^2_{obsd}$). The λ value is comparable with that for the mononuclear Eu(III) compound (472 cm^{-1}). Therefore, the magnetic behavior of **2** is mainly caused by single-ion properties, which is also reflected in the small value of the Weiss-like constant.[31]

For **3**, the observed $\chi_M T$ decreases smoothly from a value of 7.31 emu·K·mol^{-1} at 300 K to 7.25 emu·K·mol^{-1} at 30 K, and then falls sharply to 6.64 emu·K·mol^{-1} at 2 K. The $\chi_M T$ value decreases very slightly with cooling, indicating that although weak, there are some possible antiferromagnatic couplings between the neighboring Gd(III) ions. In order to estimate these magnetic interactions, the magnetic susceptibility data

dx.doi.org/10.1021/cg2008655 | Cryst. Growth Des. 2012, 12, 670−678

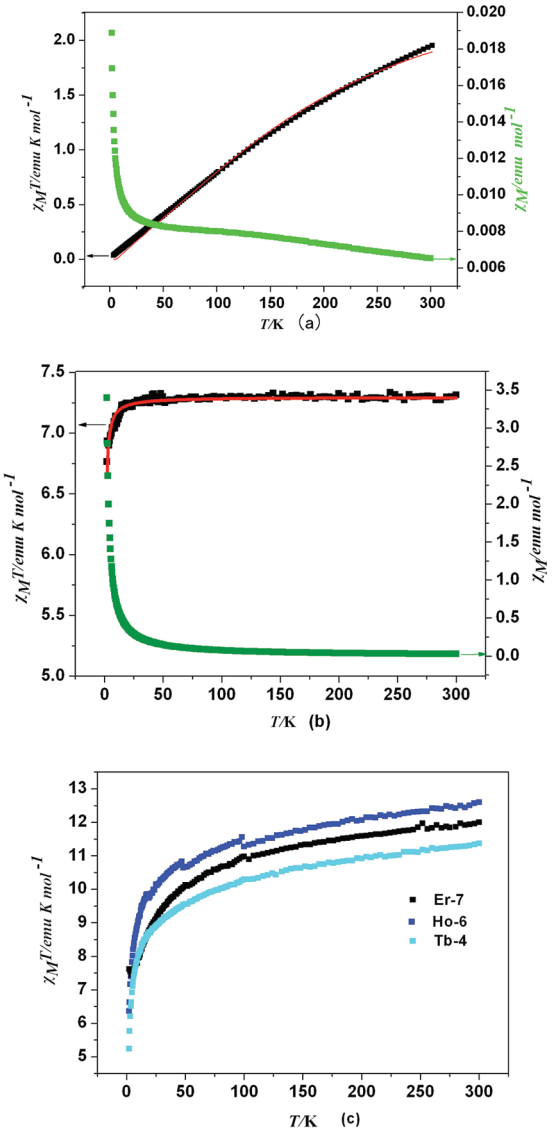

Figure 7. Temperature dependence of $\chi_M T$ and χ_M values for (a) **2**, (b) **3**, and the temperature dependence of $\chi_M T$ values for **4**, **6**, and **7** (c). The red line represents the fitting results.

were quantitatively analyzed using eq 1 based on a simple dimeric model with Hamiltonian $\mathbf{H} = -2J\mathbf{S}_A\mathbf{S}_B$ and $\mathbf{S}_A = \mathbf{S}_B = 7/2$.[32]

$$\chi_M = \frac{2Ng^2\beta^2}{kT}\frac{A}{B} \quad (1)$$

where

$$A = 140e^{56J/kT} + 91e^{42J/kT} + 55e^{30J/kT} + 30e^{20J/kT} + 14e^{12J/kT} + 5e^{6J/kT} + e^{2J/kT}$$

$$B = 15e^{56J/kT} + 13e^{42J/kT} + 11e^{30J/kT} + 9e^{20J/kT} + 7e^{12J/kT} + 5e^{6J/kT} + 3e^{2J/kT} + 1$$

and N, g, and β have their usual meanings. J is the coupling constant between the Gd(III) ions. The best fit gives $g = 1.938$, $J/K = -0.028$ cm^{-1}, and $R = 1.26 \times 10^{-4}$ (Figure 7b). The fitting results confirmed very weak antiferromagnetic coupling in the chain structure based on dinuclear units.[33]

For **5**, the observed $\chi_M T$ value at room temperature is 13.86 emu·K·mol^{-1}, which is less than the calculated value 14.26 emu·K·mol^{-1} of isolated Dy(III) ions ($g = 4/3$ $^6H_{15/2}$). Upon cooling, the $\chi_M T$ value roughly remains constant before 100 K. Below 100 K, it decreases dramatically to 9.81 emu·K·mol^{-1} at 2 K (Figure 8a). Fitting the experimental data ranging from 2 to 300K

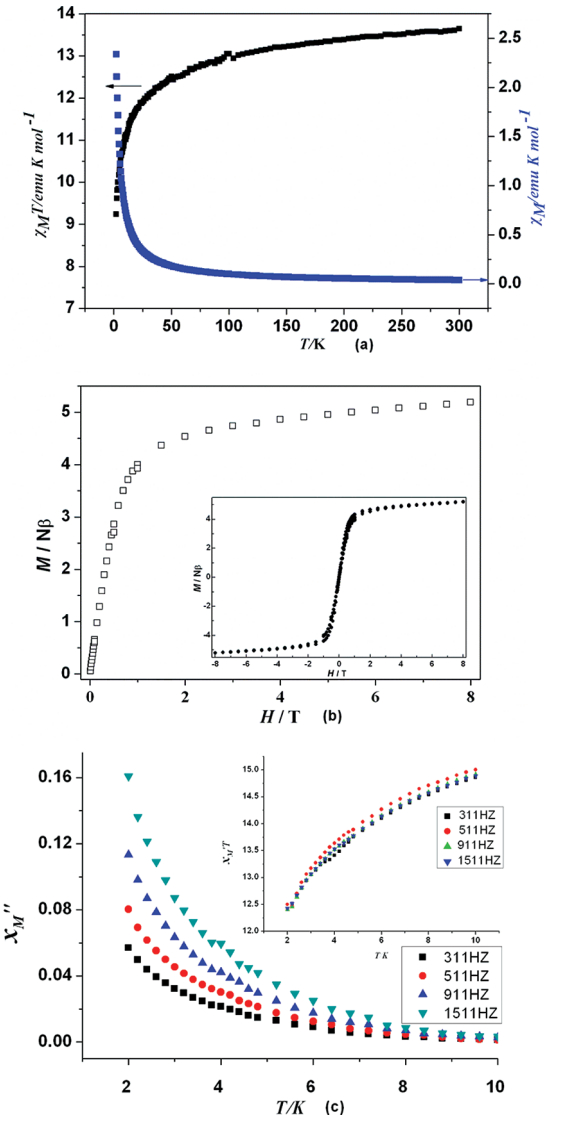

Figure 8. (a) Temperature dependence of $\chi_M T$ and χ_M values for **5**, (b) field dependence of magnetization for **5**, and (c) in-phase ($\chi'_M T$) (inset) and out-of-phase (χ''_M) AC susceptibility vs. T for **5** measured in a 3.0 G AC field oscillating at the indicated frequencies.

to Curie–Weiss law gives Curie constant $C = 14.12$ emu·mol^{-1} and Weiss constant $\theta = -0.904$ K. The negative Weiss constant suggests some antiferromagnetic interactions between spin carriers. In the M versus H plot, the maximum value of M is 5.19 μ_B at 5 T (Figure 8b), which is constant with the calculated value for one uncorrelated Dy(III) magnetic moment 5.23 μ_B. The miss of saturation on the M versus H data at 2 K suggests the presence of antiferromagnetic interaction between Dy(III) ions that make the low-lying excited states.[34] Although the M versus H plots for **5** do not show hysteresis at 2 K, the measurements of AC susceptibility under the DC field of $H_{DC} = 0$ Oe and the AC field of $H_{DC} = 3$ Oe in the temperature range of 2–10 K with a frequency from 111 to 1511 Hz shows frequency dependence.(Figure 8c).[35]

dx.doi.org/10.1021/cg2008655 | Cryst. Growth Des. 2012, 12, 670–678

For compounds **4**, **6**, and **7**, their $\chi_M T$ versus T plots present a similar behavior, where the $\chi_M T$ values decrease slowly from 300 to 2 K. The $\chi_M T$ values for **4**, **6**, and **7** are equal to 10.98, 12.87, and 11.25 emu·K·mol^{-1} at 300 K (Figure 7c), respectively, which are lower than those expected for Tb(III) (11.75 emu·K·mol^{-1}, g = 3/2, $^7F_6$), Ho(III) (14.08 emu·K·mol^{-1} g = 5/4, $^5I_8$), and Er(III) (11.48 emu·K·mol^{-1}, g = 6/5 $^4I_{15/2}$).[36] The lowering of $\chi_M T$ values with decreasing temperature can be ascribed to the depopulation of the Stark levels together with weak antiferromagnetic interactions between the lanthanide ions in **4**, **6**, and **7**. It is believed that the magnetic interaction between Er(III) ions is stronger than that between Ho(III) ions because the $\chi_M T$ value of **7** decreases more quickly than that of **6** with the temperature cooling. The magnetic susceptibility data for the plot of χ_M versus T follow Curie–Weiss behavior in the 50–300 K temperature range, with C = 10.82 emu·mol^{-1} and θ = −7.90 K for **4**, C = 13.91 emu·mol^{-1} and θ = −6.56 K for **6**, and C = 12.08 emu·mol^{-1}and θ = −8.13 K for **7**. The larger θ value of **7** compared with those of **4** and **6** also indicates that the magnetic interactions between the Ln(III) ions in **7** are stronger than those in **4** and **6**.

CONCLUSION

In summary, we have synthesized and structurally characterized a series of isostructural lanthanide-organic frameworks, Ln(TATB)(H_2O) (Ln = Y **1**, Eu **2**, Gd **3**, Tb **4**, Dy **5**, Ho **6**, and Er **7**) and investigated their thermal stabilities, gas sorption properties, luminescent behaviors, and magnetism. All these MOFs exhibit unusual thermal stability and are stable up to 550 °C in air. Gas sorption studies show that the porous framework of dehydrated **1** displays effective adsorption for CO_2, H_2, H_2O, and CH_3OH. The relatively long lifetimes and quantum yields of **2** and **4** indicate that the $TATB^{3-}$ ligand could efficiently sensitize Ln(III) ion emission. The comparison of luminescent behavior for **2** and **4** and their corresponding dehydrated samples indicates that the fluorescence quenching which arises from the H_2O-induced oscillate is very strong and fairly temperature insensitive. The variable-temperature magnetic studies for **2**–**7** suggest that magnetic interactions between the Ln(III) ions are mainly ascribed to the antiferromagnetic coupling as well as the depopulation of the Stark levels. The in-phase and out-phase signals $\chi'_M T$ and χ''_M of **5** exhibit frequency dependence.

ASSOCIATED CONTENT

Supporting Information

Tables for the selected bond lengths and angles for these compounds, plots for the XRD of **1**–**7**, emission spectra of compounds **1**, **3**, and **5**–**7** in solid state and the luminescence decay curves for **2** and **4**, and X-ray data files (CIF) are available free of charge via the Internet at http://pubs.acs.org.

AUTHOR INFORMATION

Corresponding Author

*E-mail: swdu@fjirsm.ac.cn. Fax: 86-591-83709470.

ACKNOWLEDGMENTS

We thank the financial support from the State Key Laboratory of Structural Chemistry, Fujian Institute of Research on the Structure of Matter, Chinese Academy of Sciences, National Basic Research Program of China (973 Program, 2012CB815302), the National Natural Science Foundation of China (21173221 and 20903096) for financial support.

REFERENCES

(1) (a) Li, H.; Eddaoudi, M.; O'Keeffe, M.; Yaghi, O. M. *Nature* **1999**, *402*, 276. (b) Chen, B. L.; Xiang, S. C.; Qin, G. D. *Acc. Chem. Res.* **2010**, *43*, 1115. (c) Evans, O. R.; Lin, W. B. *Acc. Chem. Res.* **2002**, *35*, 511. (d) Chen, B; Eddaoudi, M; Hyde, S. T.; O'Keeffe, M.; Yaghi, O. M. *Science* **2001**, *291*, 1021. (e) Lee, S. J.; Lin, W. B. *Acc. Chem. Res.* **2008**, *41*, 521. (f) Chen, X. M.; Tong, M. L. *Acc. Chem. Res.* **2007**, *40*, 162. (g) Wang, F.; Liu, Z. S.; Yang, H.; Tan, Y. X.; Zhang, J. *Angew. Chem., Int. Ed.* **2011**, *50*, 450. (h) Cui, Y. J.; Yue, Y. F.; Qian, G. D.; Chen, B. L. *Chem. Rev.* **2011**, DOI: 10.1021/cr200101d.

(2) (a) Carlucci, L.; Ciani, G.; Proserpio, D. M. *Coord. Chem. Rev.* **2003**, *246*, 247. (b) James, S. L. *Chem. Soc. Rev.* **2003**, *32*, 276. (c) Kitaura, R.; Seki, K.; Akiyama, G.; Kitagawa, S. *Angew. Chem., Int. Ed.* **2003**, *42*, 428. (d) Lo, S. M-F.; Chui, S. S Y.; Shek, L. Y.; Lin, Z. Y.; Zhang, X. X.; Wen, G. H; Williams, I. D. *J. Am. Chem. Soc.* **2000**, *122*, 6293. (e) Eddaoudi, M.; Kim, J.; Rosi, N.; Vodak, D.; Wachter, D. V.; O'Keeffe, M.; Yaghi, O. M. *Science* **2002**, *295*, 469. (f) Wang, C.; Lin, W. B. *J. Am. Chem. Soc.* **2011**, *133*, 4232. (g) Ockwig, N. W.; Delgado, F. O.; O'Keeffe, M.; Yaghi, O. M. *Acc. Chem. Res.* **2005**, *38*, 176. (h) Chen, B. L.; Wang, L. B.; Xiao, Y. Q.; Fronczek, F R.; Xue, M.; Cui, Y. J.; Qian, G. D. *Angew. Chem., Int. Ed.* **2009**, *48*, 500.

(3) (a) Zheng, S. L.; Tong, M. L.; Chen, X. M. *Coord. Chem. Rev.* **2003**, *246*, 185. (b) Bu, X. H.; Tong, M. L.; Chang, H. C.; Kitagawa, S.; Batten, S. R. *Angew. Chem., Int. Ed.* **2004**, *43*, 192. (c) Zheng, Y. Z.; Tong, M. L.; Zhang, W. X.; Chen, X. M. *Angew. Chem., Int. Ed.* **2006**, *45*, 6310. (d) Li, C. J.; Lin, Z. J.; Peng, M. X.; Leng, J. D.; Yang, M. M.; Tong, M. L. *Chem. Commun.* **2008**, 6348. (e) He, Q. T.; Li, X. P.; Liu, Y.; Yu, Z. Q.; Wang, W.; Su, C. Y. *Angew. Chem., Int. Ed.* **2009**, *48*, 6156. (f) Zeng, Y. F.; Hu, X.; Liu, F. C.; Bu, X. H. *Chem. Soc. Rev.* **2009**, *38*, 469. (g) Chen, B. L.; Yang, Y.; Zapata, F.; Lin, G.; Qian, G.; Lobkovsky, E. B. *Adv. Mater.* **2007**, *19*, 1693.

(4) (a) Peng, G.; Ma, L.; Cai, J. B.; Liang, L.; Deng, H.; Kostakis, G. E. *Cryst. Growth Des.* **2011**, *11*, 2485. (b) Yang, W. B.; Greenaway, A.; Lin, X.; Matsuda, R.; Blake, A. J.; Wilson, C.; Lewis, W.; Hubberstey, P.; Kitagawa, S.; Champness, N. R.; Schröder, M. *J. Am. Chem. Soc.* **2010**, *132*, 14457. (c) Wang, S. N.; Xing, H.; Li, Y. Z.; Bai, J. F.; Scheer, M.; Pan, Y.; You, X. Z. *Chem. Commun.* **2007**, 2293. (d) Chen, B. L.; Wang, L.; Zapata, F.; Qian, G.; Lobkovsky, E. *J. Am. Chem. Soc.* **2008**, *130*, 6718. (e) Guo, Z. Y.; Xu, H.; Su, S. Q.; Cai, J. F.; Dang, S.; Xiang, S. C.; Qian, G. D.; Zhang, H. J.; O'Keeffe, M.; Chen, B. L. *Chem. Commun.* **2011**, *47*, 5551.

(5) (a) Xue, D. X.; Lin, J. B.; Zhang, J. P.; Chen, X. M. *CrystEngComm* **2009**, *11*, 183. (b) Gao, Q.; Jiang, F. L.; Wu, M. Y.; Huang, Y. G.; Wei, W.; Hong, M. C. *Cryst. Growth Des.* **2010**, *10*, 184. (c) Yang, A, H.; Zhao, L, H.; Quan, Y, P.; Gao, H. L.; Cui, J. Z.; Shi, W.; Cheng, P. *Cryst. Growth Des.* **2010**, *10*, 218.

(6) (a) Wu, M. F.; Wang, M. S.; Guo, S. P.; Zheng, F. K; Chen, H. F.; Jiang, X. M.; Liu, G. N.; Guo, G. C.; Huang, J. S. *Cryst. Growth Des.* **2011**, *11*, 372. (b) Gao, H. L.; Yi, L.; Ding, B.; Wang, H. S.; Cheng, P.; Liao, D. Z.; Yan, S. P. *Inorg. Chem.* **2006**, *45*, 481. (c) Khasnis, D.; Brewer, V. M.; Lee, T.; Enge, T. J.; Brennan, J. G. *J. Am. Chem. Soc.* **1994**, *116*, 7129. (d) Chen, B. L.; Yang, Y.; Zapata, F.; Qian, G. D.; Luo, Y. S.; Zhang, J. H.; Lobkovsky, E. B. *Inorg. Chem.* **2006**, *45*, 8882. (e) Chen, M. C.; Li, L. H.; Chen, Y. B.; Chen, L. *J. Am. Chem. Soc.* **2011**, *133*, 4617. (f) Han, L. W.; Lü, J.; Liu, T. f.; Gao, S. Y.; Cao, R. *Dalton Trans.* **2010**, *39*, 10967.

(7) (a) Bernot, K.; Bogani, L.; Caneschi, A.; Gatteschi, D.; Sessoli, R. *J. Am. Chem. Soc.* **2006**, *128*, 7947. (b) Sun, Y, Q.; Zhang, J.; Chen, Y. M.; Yang, G, Y. *Angew. Chem., Int. Ed.* **2005**, *44*, 5814. (c) Kobayashi, A.; Suzuki, Y.; Ohba, T.; Noro, S. I.; Chang, H. C.; Kato, M. *Inorg. Chem.* **2011**, *50*, 2061. (d) Xu, Q. H.; Li, L. S.; Liu, X. S.; Xu, R. R. *Chem. Mater.* **2002**, *14*, 549. (e) Chauvin, A. S.; Comby, S.; Band, M.; Piano, C. D.; Duhot, C.; Bünzli, J. C. G. *Inorg. Chem.* **2009**, *48*, 10687. (f) Kerbellec, N.; Kustaryono, D.; Haquin, V.; Etienne, M.; Daiguebonne, C.; Guillou, O. *Inorg. Chem.* **2009**, *48*, 2837.

(8) (a) Ma, S. Q.; Wang, X. S.; Yuan, D. Q.; Zhou, H. C. *Angew. Chem., Int. Ed.* **2008**, *47*, 4130. (b) Lill, D. T.; Cahill, C. L. *Chem. Commun.* **2006**, 4946.
(9) Jiang, H. L.; Tsumori, N.; Xu, Q. *Inorg. Chem.* **2010**, *49*, 10001.
(10) (a) Sun, D.; Ma, S.; Ke, Y.; Collins, D. J.; Zhou, H. C. *J. Am. Chem. Soc.* **2006**, *128*, 3896. (b) Ma, S.; Sun, D.; Ambrogio, M. W.; Fillinger, J. A.; Parkin, S.; Zhou, H. C. *J. Am. Chem. Soc.* **2007**, *129*, 1858.
(11) (a) Sun, D.; Ma, S.; Ke, Y.; Petersen, T. M.; Zhou, H. C. *Chem. Commun.* **2005**, 2663. (b) Sun, D. F.; Ke, Y.; Collins, D. J.; Lorigan, G. A.; Zhou, H. C. *Inorg. Chem.* **2007**, *46*, 2725. (c) Yu, C.; Ma, S.; Pechan, M. J.; Zhou, H. C. *J. Appl. Phys.* **2007**, *101*, 09E108.
(12) Ma, S.; Wang, X. S.; Manis, E. S.; Collier, C. D.; Zhou, H. C. *Inorg. Chem.* **2007**, *46*, 3432.
(13) Ma, S.; Zhou, H. C. *J. Am. Chem. Soc.* **2006**, *128*, 11734.
(14) Sheldrick, G. M. *SADABS*; University of Göttingen: Göttingen, Germany, 1996.
(15) *SHELXTL* (version 5.10); Siemens Analytical X-ray Instruments Inc.: Madison, WI, 1994.
(16) Noveron, J. C.; Lah, M. S.; Del Sesto, R. E.; Arif, A. M.; Miller, J. S.; Stang, P. J. *J. Am. Chem. Soc.* **2002**, *124*, 6613.
(17) (a) Qiu, Y. C.; Deng., H.; Yang., S. H.; Mou, J. X.; Daiguebonne, C.; Kerbellec, N.; Guillou, O; Batten, S. R. *Inorg. Chem.* **2009**, *48*, 3976. (b) Xu, X. X.; Zhang, Xia.; Liu, X. X.; Sun, T.; Wang, E. B. *Cryst. Growth Des.* **2010**, *10*, 2272.
(18) (a) Blake, A. J.; Champness, N. R.; Hubberstey, P.; Li, W. S.; Withersby, M. A.; Schröder, M. *Coord. Chem. Rev.* **1999**, *183*, 117. (b) Batten, S. R; Hoskins, B. F.; Robson, R. *Chem.—Eur. J* **2000**, *6*, 156. (c) Carlucci, L.; Cozzi, N.; Ciani, G.; Moret, M.; Proserpio, D. M.; Rizzato, S. *Chem. Commun.* **2002**, 1354. (d) Moulton, B.; Lu, J. J.; Zaworotko, M. J. *J. Am. Chem. Soc.* **2001**, *123*, 9224. (e) Feng, R.; Jiang, F. L.; Chen, L.; Yan, C. F.; Wu, M. Y.; Hong, M. C. *Chem. Commun.* **2009**, 5296.
(19) (a) Yang, S. Y.; Long, L. S.; Jiang, Y. B.; Huang, R. B.; Zheng, L. S. *Chem. Mater.* **2002**, *14*, 3229. (b) Banerjee, D.; Borkowski, L. A.; Kim, S. J.; Parise, J. B. *Cryst. Growth Des.* **2009**, *9*, 4922.
(20) (a) Furukawa., H.; Miller, M. A.; Yaghi., O. M. *J. Mater. Chem.* **2007**, *17*, 3197. (b) Zhang, H. X.; Wang, F.; Yang, H.; Tan, Y. X.; Zhang, J; Bu, X. H. *J. Am. Chem. Soc.* **2011**, *133*, 11884.
(21) (a) Sudik, A.; Côté, A. P.; Wong-Foy, A.; O'Keeffe, M.; Yaghi, O. M. *Angew. Chem., Int. Ed.* **2006**, *45*, 2528. (b) Loiseau, T.; Lecroq, L.; Volkringer, C.; Marrot, J.; Férey, G.; Haouas, M.; Taulelle, F.; Bourrelly, S.; Llewellyn, P. L.; Latroche, M. *J. Am. Chem. Soc.* **2006**, *128*, 10223.
(22) (a) Zhong, D. C.; Lin, J. B.; Lu, W. G.; Jiang, L.; Lu, T. B. *Inorg. Chem.* **2009**, *48*, 8656. (b) Choi, H. S.; Suh, M. P. *Angew. Chem., Int. Ed.* **2009**, *48*, 6865. (c) Liu, T. F.; Lu, J.; Lin, X; Cao, R. *Chem. Commun.* **2010**, 8439.
(23) (a) Vishnyakov, A.; Ravikovitch, P. I.; Neimark, A. V.; Bulow, M.; Wang, O. M. *Nano Lett.* **2003**, *3*, 713. (b) Lee, J. Y.; Jagiello, J. *J. Solid State Chem.* **2005**, *178*, 2527.
(24) (a) Belof, J. L.; Stern, A. C.; Eddaoudi, M.; Space, B. *J. Am. Chem. Soc.* **2007**, *129*, 15202. (b) Frost, H.; Dren, T.; Snurr, R. Q. *J. Phys. Chem. B.* **2006**, *110*, 9565. (c) Li, J.; Furuta, T.; Goto, H.; Ohashi, T.; Fujiwara, Y.; Yip, S. *J. Chem. Phys.* **2003**, *119*, 2376. (d) Nechaev, Y. S.; Alexeeva, O. K. *Int. J. Hydrogen Energy* **2003**, *28*, 1433.
(25) (a) Zhong, D. C.; Lin, J. B.; Lu, W. G.; Jiang, L.; Lu, T. B. *Inorg. Chem.* **2009**, *48*, 8656. (b) Zhang, J.; Xue, Y. S.; Liang, L. L.; Ren, S. B.; Li, Y. Z.; Du, H. B.; You, X. Z. *Inorg. Chem.* **2010**, *49*, 7685.
(26) (a) Judd, R. *Phys. Rev.* **1962**, *127*, 750. (b) Ofelt, G. S. *J. Chem. Phys.* **1962**, *37*, 511.
(27) (a) Chen, X. Y.; Zhao, W.; Cook, R. E.; Liu, G. K. *Phys. Rev. B* **2004**, *70*, 205122. (b) Chen, X .Y.; Liu, G. K. *J. Solid State Chem.* **2005**, *178*, 419.
(28) (a) Huang, Y.; Song, Y. S.; Yan, B.; Shao, M. *J. Solid State Chem.* **2008**, *181*, 1731. (b) Bauer, C. A.; Timofeeva, T. V.; Settersten, T. B.; Patterson, B. D.; Liu, V. H.; Simmons, B. A.; Allendorf, M. D. *J. Am. Chem. Soc.* **2007**, *129*, 7136.
(29) (a) Stein, G.; Wurzburg, E. *J. Chem. Phys.* **1975**, *62*, 208. (b) Dew, W., H. Jr.; Sudnick, D. R. *J. Am. Chem. Soc.* **1979**, *101*, 334. (c) Liu, T. F.; Zhang, W. J.; Sun, W. H.; Cao, R. *Inorg. Chem.* **2011**, *50*, 5242. (d) Richardson, F. S. *Chem. Rev.* **1982**, *82*, 541.
(30) Gorller-Warland, C.; Binnemans, K. In *Handbook on the Physics and Chemistry of the Rare Earths*; Gschneidner, Jr., K. A.; Eyring, L., Eds.; North-Holland: Amsterdam, 1998; Vol. *25*, pp 220–221.
(31) Andruh, M.; Bakalbassis, E.; Kahn, O.; Trombe, J. C.; Porcher, P. *Inorg. Chem.* **1993**, *32*, 1616.
(32) (a) Panagiotopoulos, A.; Zafiropoulos, T. F.; Perlepes, S. P.; Bakalbassis, E.; Masson-Ramade, I.; Kahn, O.; Terzis, A.; Raptopoulou, C. P. *Inorg. Chem.* **1995**, *34*, 4918. (b) Costes, J. P.; Clemente-Juan, J. M.; Dahan, F.; Nicodème, F.; Verelst, M. *Angew. Chem., Int. Ed.* **2002**, *41*, 323.
(33) (a) John, D.; Urland, W. *Eur. J. Inorg. Chem.* **2006**, 3503. (b) Rohde, A.; Urland, W. *Dalton Trans.* **2006**, 2974.
(34) (a) Hatfield, W. E. *J. Appl. Phys.* **1981**, *52*, 1985. (b) Cortés, R.; Drillon, M.; Solans, X.; Lezama, L.; Rojo, T. *Inorg. Chem.* **1997**, *36*, 677.
(35) (a) Kajiwara, T.; Nakano, M.; Kaneko, Y.; Takaishi, S.; Ito, T.; Yamashita, M.; Igashira-Kamiyama, A.; Nojiri, H.; Ono, Y.; Kojima, N. *J. Am. Chem. Soc.* **2005**, *127*, 10150. (b) Costes, J. P.; Clemente-Juan, J. M.; Dahan, F.; Milon, J. *Inorg. Chem.* **2004**, *43*, 8200. (c) Pardo, E.; Ruiz- Garcia, R.; Lloret, F.; Faus, J.; Julve, M.; Journaux, Y.; Delgado, F.; Ruiz-Perez, C. *Adv. Mater* **2004**, *16*, 1597.
(36) (a) Chen, W.; Wang, J. Y.; Chen, C.; Yue, Q.; Yuan, H. M.; Chen, J. S.; Wang, S. N. *Inorg. Chem.* **2003**, *42*, 944. (b) Thirumurugan, A.; Natarajan, S. *Dalton Trans.* **2004**, 2923.